

# Nonlinear modeling of cyclic response of RC beam–column joints reinforced by plain bars

Mahdi Adibi<sup>1</sup>  · Mohammad S. Marefat<sup>2</sup> · Reza Allahvirdizadeh<sup>3</sup>

Received: 27 December 2017 / Accepted: 22 May 2018 / Published online: 28 May 2018  
© Springer Science+Business Media B.V., part of Springer Nature 2018

**Abstract** Experience of previous earthquakes shows that a considerable portion of buildings reinforced with plain bars sustain relatively large damages especially at the beam–column joints where the damages are mostly caused by either diagonal shear cracks or intersectional cracks caused by bar slippage. While previous works mainly focus on shear failure mode, in this study, the emphasis is placed on slip based cracks as the dominant failure mode. A systematic procedure is introduced to predict the dominant failure mode at the joint which is based on the dimensional properties, reinforcement details, and axial and shear load at the joint. In addition, a relatively simple and efficient nonlinear model is proposed to simulate pre- and post-elastic behavior of the joints which fail under bar slippage mode. In this model, beam and column components are represented by linear elastic elements, dimensions of the joint panel are defined by rigid elements, and effect of slip is taken into account by a nonlinear rotational spring at the end of the beam. The proposed method is validated by experimental results for both internal and external joints .

**Keywords** Seismic assessment · Nonlinear modeling · Exterior and interior beam–column joints · Plain bars

---

✉ Mahdi Adibi  
m.adibi@ub.ac.ir; mahdi.adibi@gmail.com

Mohammad S. Marefat  
mmarefat@ut.ac.ir

Reza Allahvirdizadeh  
allahvirdizadeh@gmail.com; allahvirdizadeh@civil.uminho.pt

<sup>1</sup> Earthquake Engineering, School of Civil Engineering, University of Bojnord, Bojnord, Iran

<sup>2</sup> Structural Engineering, School of Civil Engineering, University of Tehran, Tehran, Iran

<sup>3</sup> ISISE, Department of Civil Engineering, University of Minho, Guimarães, Portugal

## 1 Introduction

Obtained experiences from previous earthquakes showed significant seismic vulnerability of existing reinforced concrete buildings, particularly those which were constructed prior to 1970s. It motivated researchers to develop advanced evaluation methods and upgrade ongoing assessment tools (Allahviridzadeh and Mohammadi 2016). These buildings were designed mainly by taking gravity actions into account. Thus, modern design regulations with respect to the lateral loads, e.g. strong joint panels and weak beam–strong column have not been considered in their design process (Park et al. 1995; Sezen et al. 1999, 2003; ATC 1989; Hakuto et al. 1995). In addition to such deficiencies, it was typical during the 1950–1970s to adopt plain bars as reinforcement instead of deformed ones, add no stirrups to the joint region, use concretes with low compressive strength and not provide sufficient anchorage for longitudinal reinforcements (Bedirhanoglu et al. 2010; Yurdakul and Avsar 2016; Del Vecchio et al. 2017). All aforementioned weaknesses led them to present a poor seismic performance; which causes them to damage severely under earthquakes with much less intensity than expected from modern buildings to withstand. Hence, recognizing their possible failure modes, developing reliable methods to predict their response and proposing efficient strengthening solutions to enhance their responses received a great attention during recent years.

Conducted experimental investigations on RC subassemblies reinforced by deformed bars introduced shear and bond deterioration as the most widely observed failure modes. These failures occur by developing diagonal cracks in the joint panel which follows by reduction in strength/stiffness and increase in the experienced story drift ratio (Hakuto et al. 1999; Manfredi et al. 2008; Soleimani et al. 1979). In contrary of that, the possible failure mode of RC structures reinforced by plain bars is observed as sliding of reinforcements. Such failure prevents adjacent beams to reach their flexural capacity (i.e. plastic hinge formation in the beams as it is expected from modern buildings) and joints to experience shear cracks (Bedirhanoglu et al. 2010; Pampanin et al. 2000, 2003; Calvi and Pampanin 2002; Liu and Park 2000, 2001; Russo and Pauletta 2012; Braga et al. 2009; Cosenza and Prota 2006). It should be noted that the transformation mechanism of shear stress in the joints without transverse reinforcement is mainly dependent on the formed compression strut due to initiation of diagonal crack, which is evidently a function of confinement level of the joint (Pampanin et al. 2006). Hence, a different behavior (from hysteresis, hardening and strength point of view) should be expected from interior joints with respect to exterior ones (Calvi and Pampanin 2002).

Considering aforementioned behaviors, it seems hardly possible for the current assessment methods to predict reliably the seismic response of the old-fashioned RC buildings reinforced with plain bars. Additionally, proposing effective strengthening solutions in the practical projects without adopting such assessment tools would be a cumbersome task. It is evident that these methods should be able to capture not only the local behaviors, including that of the joints, beams, and columns but also should precisely represent the global response.

In this regard, several modeling strategies have been proposed in the literature. Conventionally, beam–column joints are modeled using rigid elements (see Fig. 1a). This assumption leads to reasonable outcomes for modern structures subjected to ground motions with low/moderate intensity, but it generally overestimates the stiffness (underestimates experienced lateral displacements) of the existing buildings and misleadingly predicts their failure mechanisms (Manfredi et al. 2008; Hakuto et al. 2000). Moreover, this method cannot

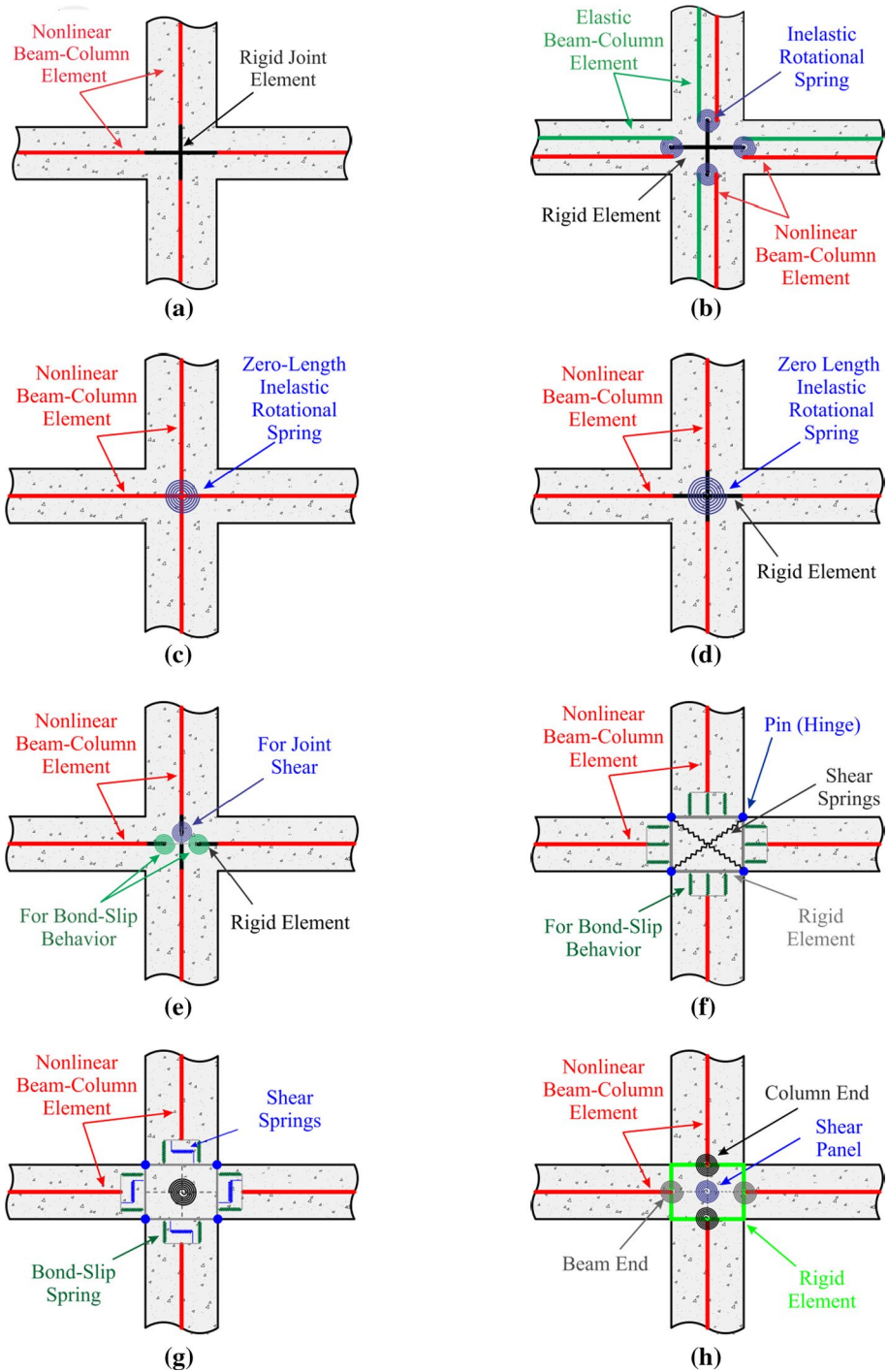


**Fig. 1** Different joint modeling approaches. **a** conventional rigid joint, **b** Otani (1974), **c** El-Metwally and Chen (1988), **d** Alath and Kunnath (1995), **e** Biddah and Ghobarah (1999), **f** Yousef and Ghobarah (2001), **g** Lowles and Altoontash (2003), **h** Altoontash (2004)

predict shear deformations, diagonal cracking and bond loss (rebar slippage) which was widely observed even in modern buildings under strong earthquakes, and it was shown that have a significant contribution on experienced lateral displacements (Manfredi et al. 2008; Allahvirdizadeh and Gholipour 2017; Allahvirdizadeh et al. 2017). This inaccurate consideration of strength and ductility by rigid element approach (Park 2002) led more detailed modeling techniques to be proposed.

For instance, ASCE/SEI 41 and FEMA-356 model the geometry of the joint by following the same rigid element approach; however, an empirical backbone curve is introduced to consider its shear deformations (ASCE, SEI 41 2007; FEMA-356 2000). Similarly, this method also overestimates the stiffness of the building. Therefore, Giberson has proposed assigning a nonlinear rotation spring to each end of the beam–column elements. In this method, the linear elastic elements were used for the beams and columns; hence assigned springs represent both nonlinear deformations of beams (flexural) and joint (shear) (Giberson 1969). These linear beam–column elements were later replaced by two parallel elements (which one was for representing linear elastic behavior, and the other one was for post-elastic behavior) by Otani. In this method, the dimension of the joint is again modeled by rigid elements, and rotational springs were introduced into the interface of joint and adjacent components to consider bar slippage (see Fig. 1b) (Otani 1974). In the following, the behavior of the joint was decoupled from that of the beam/column by assigning a zero-length element (rotational spring) at its midsection. It is worthwhile to note that some of these methods take into account the dimension of the joint by rigid links, whereas the others continue beam–column elements and directly connect them to the joint spring (Fig. 1c, d) (El-Metwally and Chen 1988; Alath and Kunnath 1995). Later, this model was modified by substituting the single spring with a group of springs in series; which can separately consider shear deformations of the joint and bar slippage (Fig. 1e) (Biddah and Ghobarah 1999). A relatively same model was proposed by Yousef and Ghobarah; whereas they used diagonal shear springs to connect the hinges at corners of the joint. These hinges were horizontally connected to each other by rigid elements, and bar-slip springs were added at the intersection of each beam/column with the joint (Fig. 1f) (Youssef and Ghobarah 2001). The same approach is followed by Lowes and Altoontash, which is schematically depicted in Fig. 1g (Lowes and Altoontash 2003). As it is clear, a variety of parameters are required to be defined in each joint zone, which makes its application to be a complicated task. Therefore, a simplified model was developed by Altoontash (2004), which interface springs (consisted of twelve springs for an interior joint) were replaced by four rotational springs (Fig. 1h). It is worthwhile to note that in spite of all achieved progresses in consideration of joint behavior on seismic behavior of RC buildings, the influence of the smooth bar is still not well addressed and understood.

Minor studies have been focused particularly on the seismic response of old-fashioned RC structures, i.e. those which were only designed to withstand gravity loads and reinforced by plain bars. Among which Pampanin et al. (2000) and Calvi et al. (2001, 2002) carried out an experimental investigation on RC subassemblies and three-story frame, representing Italian construction practice during the 1950s until 1970s. Obtained outcomes led them to propose an empirical shear behavior to be assigned to the joint. Their proposed model is relatively similar to that of Alath and Kunnath (see Fig. 1d), i.e. the joint geometry is modeled by rigid elements, and an equivalent rotational spring is added to the midsection. Characteristics of this moment-rotational spring are derived by considering the equilibrium between principal tensile stress and shear deformation; which can be obtained by considering the contraflexure points of adjacent beams/columns at their mid-span and assuming principal tensile stress at the crack initiation point of the joint to be equal to

$0.2\sqrt{f'_c}$  and  $0.4\sqrt{f'_c}$  respectively for exterior and interior joints. Additionally, a perfectly plastic post-elastic behavior was considered for exterior joints; however, a hardening up to  $0.42\sqrt{f'_c}$  principal tensile stress was proposed for interior joints. Regarding the nonlinear behavior of beams and columns, concentrated plasticity approach is employed by assigning rotational springs at their intersections with the joint (Calvi and Pampanin 2002). A relatively same approach is followed by Laterza et al., who conducted an experimental study on both internal and external non-ductile beam–column connections built to be consistent with Italian practice during 1950–1970s. The observed damage patterns include forming diagonal shear cracks within the joint region and slippage of the longitudinal bars. Hence, they proposed a nonlinear modeling technique, which considers the geometry of the joint using rigid elements and assigns an elastic-perfectly plastic bond stress-slip relationship to diagonal shear springs (Laterza et al. 2017). Aforementioned bond-slip model is proposed by Braga et al., which assumes a linear bond-slip field along the bar, and any anchorage at its end is taken into account by a linear function of displacement (Braga et al. 2012). Such assumptions avoid conducting conventional iterative procedures, which its accuracy was validated for both poor and modern detailed components (D’Amato et al. 2012).

As discussed, the aforementioned model is valid for the joints which their failure mode includes diagonal shear crack; while some other RC subassemblies reinforced with plain rebars may fail due to developing cracks at the intersection of the adjacent beam and the joint. Hence, in the current article, an innovative joint model is proposed to capture reliably the post-elastic behavior of such components. In this regard, previously collected database, including dimensions and reinforcement details of more than 70 existing RC buildings (constructed during the 1970s and located in Tehran, Iran) were employed to design an extensive experimental program on old-fashioned RC subassemblies (Marefat et al. 2005, 2006). This program consists of both interior and exterior joints (Adibi et al. 2017a, b). In the following, outcomes of these tests were adopted to propose an empirical rotational spring model. This approach is validated by constructing nonlinear models of the tested specimens in OpenSees software framework (OpenSees 2013); which revealed accuracy and reliability of the proposed model.

It is worthwhile to note that only 2D behavior of subassemblies is taken into account, since there were no reliable experimentally captured responses and also for the sake of simplicity. Hence, influences of 3D response—e.g. multiaxial bending, torsion and higher confinement level of the joint are neglected.

## 2 Considered old-fashioned RC subassemblies

In this study, seismic behavior of old-fashioned interior and exterior joints are investigated. Geometric and detailing specifications are obtained from surveyed typical RC buildings constructed prior to the 1970s in Tehran, Iran. Usually, their story height and effective beam span length are 2.9 and 5.5 m, respectively. It should be noted that, buildings with almost similar details according the old design codes and references may be found in other countries such as Italy, Portugal and Turkey (Taylor et al. 1925; Duhman 1953; Pernot 1954; Guerrin 1959; Barker 1979; Edvard and Tanner 1996).

As previously mentioned, the main deficiencies of the non-seismically designed beam–column joints are usage of plain bars, absence of transverse hoops, strong beam–weak column, and insufficient anchorage condition of longitudinal reinforcements.

Generally, the anchorage length of the longitudinal beam bars equals to the effective width of the joint with  $180^\circ$  hooks.

In the following, this database is employed to design an extensive experimental program by constructing specimens consistent with practice conditions of the desired period, which are detailed in Fig. 2 and Table 1. The experimental program consisted of applying reverse-cyclic quasi-static unidirectional loading on three half scale exterior (denoted hereafter as SC1 and SC1-1) and interior (called as SC2) RC beam–column joints. Dimensions and reinforcement of the beam and column in the interior joint are identical to the exterior joints. The cross section dimensions of the columns and beams are  $250 \times 250$  mm and  $200 \times 300$  mm, respectively. Regarding the reinforcement,  $4\Phi 14$  ( $\rho_{\text{col}}=1\%$ ), and  $\Phi 6.5@160$  mm plain bars are used respectively for longitudinal reinforcement of the column and transverse reinforcement at the outside of the joint panel zone.

Moreover, it should be noted that a constant axial load ratio equal to the 7% of the section capacity ( $0.07A_g f'_c$ ) is applied to SC1 and SC2; however, the SC1-1 subassembly undergoes an axial load of about 15% of adjacent column's capacity ( $0.15A_g f'_c$ ). In sum, the nomenclatures used for the various test specimens are presented in Table 1. Additionally, the mechanical properties of the steel reinforcement and the compressive strength of the concrete specimens at the age of testing are presented in Tables 2 and 3, respectively.

The test setup is illustrated in Fig. 3. Lateral cyclic loading with increasing amplitudes is quasi-statically applied at the top of the column by a hydraulic actuator with a  $\pm 100$  kN loading capacity and a  $\pm 200$  mm displacement range. Furthermore, a vertical  $\pm 250$  kN capacity hydraulic jack was used to apply a constant axial load to the column through a link beam. For each specimen, a total of 10 electrical resistance strain gauges were attached to longitudinal and transverse reinforcements at critical sections and 13 linear variable displacement transducers (LVDTs) were used to record the deformation of the beam/column and distortions of the joint. Additionally, the positive/negative loading directions and provided boundary conditions are indicated in Fig. 3.

### 3 Experimentally observed seismic response of substructures

#### 3.1 Exterior beam–column joints (SC1 and SC1-1)

The initiation and development process of the flexural cracks in exterior joints at different loading stages are illustrated Figs. 4 and 5. It was observed that the cracks initially formed at very low drift ratios (of about 0.45%) at two sections of the beam (one at its intersection with the column and the other at a distance of 37 cm from the joint). In the following, additional flexural cracks appeared at higher lateral displacements over the zone where longitudinal bars were bent (see Fig. 2a). It is worthwhile to note that cracking was observed neither within the joint region nor in the column during the elastic range of the behavior.

These cracks with maximum width of about 5 mm at the intersection of the joint were relatively stabilized at drift ratios beyond 1.35%; nevertheless, the observed damages shifted to the rocking behavior and cover spalling at the joint region. In the following (at a drift ratio of about 1.8%), cracks parallel to the longitudinal bars and diagonal cracks developed over the beam and in the joint panel zone, respectively. Finally, at a drift ratio of 2.7%, concrete wedge spalling at the exterior face of the joint was observed, which ended by X-shape cracks, concrete wedge spalling and crushing at a drift ratio of about 3.65%.

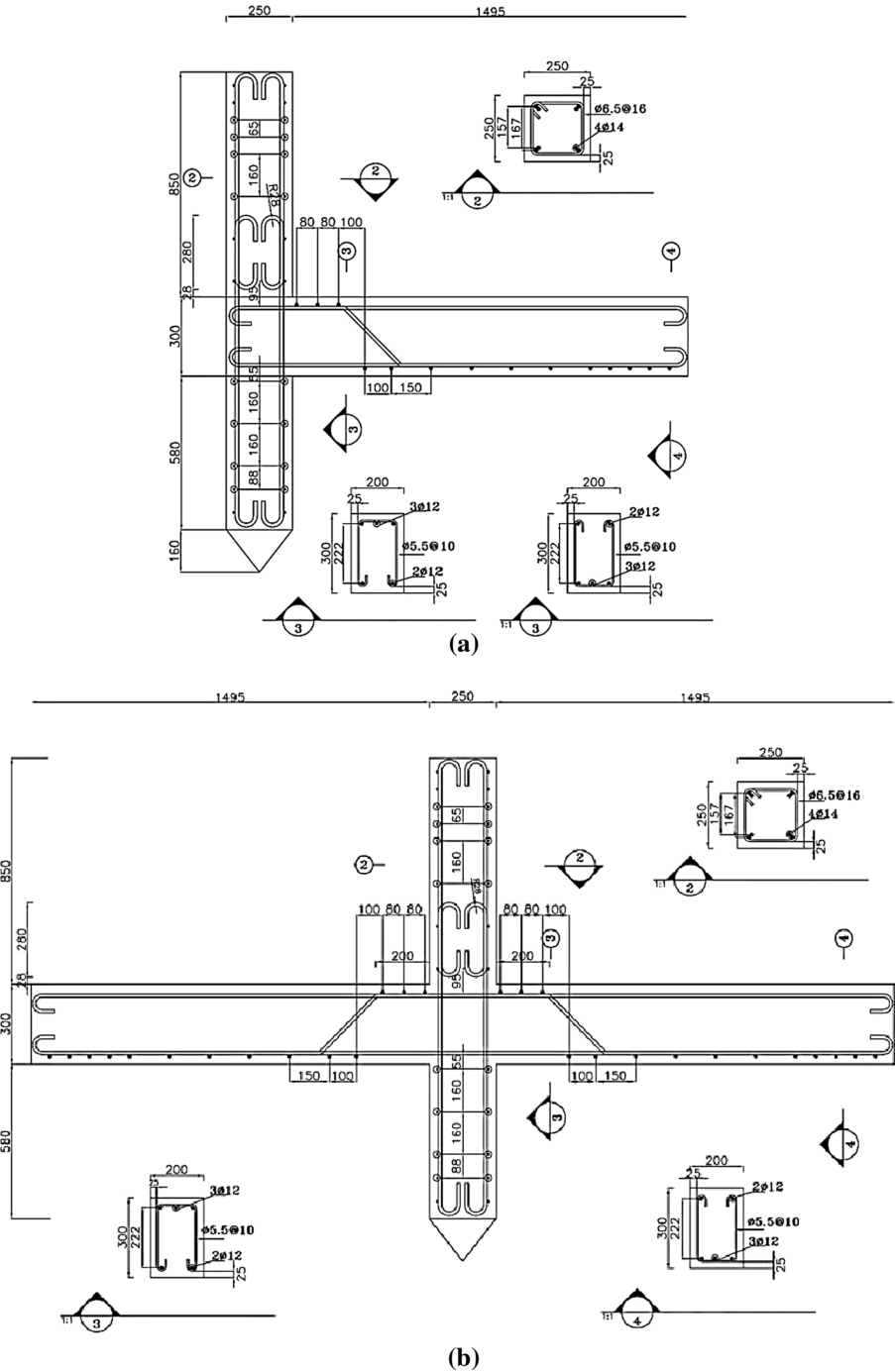


**Fig. 2** Dimensions and reinforcement details of the tested joint subassemblies. **a** Exterior beam–column joint specimen (SC1 and SC1-1). **b** Interior beam–column joint specimen (SC2)

**Table 1** Schedule of test specimens

Specimen	$P/A_g f'_c$	Loading	Column		Beam			Specification
			$\rho_{col}$	$A_v/s$ (mm)	$\rho_{top}$	$\rho_{bot}$	$A_v/s$ (mm)	
SC1	0.07	Cyclic	0.01	0.396	0.0057	0.0038	0.32	Exterior joint
SC1-1	0.15	Cyclic	0.01	0.396	0.0057	0.0038	0.32	Exterior joint
SC2	0.07	Cyclic	0.01	0.396	0.0057	0.0038	0.32	Interior joint

$A_g$ : gross sectional area,  $f'_c$ : standard cylinder compressive strength of concrete,  $A_s$ : cross-sectional area of each stirrup,  $s$ : spacing of stirrups,  $\rho$ : longitudinal reinforcement ratio

**Table 2** Mechanical properties of reinforcement bars

Bar diameter (mm)	Position	Yield strength (MPa)	Ultimate strength (MPa)	Yield strain ( $\epsilon_y$ )	Ultimate strain ( $\epsilon_{max}$ )
5.5	Beam stirrup	340	470	0.0012	0.28
6.5	Column stirrup	224	336	0.0013	0.25
12	Beam longitudinal bars	360	500	0.0015	0.28
14	Column longitudinal bars	320	450	0.0017	0.30

$\epsilon_{max}$ : strain at which fracture occurs

**Table 3** Compressive strength of concrete for different specimens

Specimen	Compressive strength (MPa)
SC1	23.6
SC1-1	22.5
SC2	23.6

On the other hand, the SC1 specimen reached its nominal flexural capacity in pull direction (the weak face of the beam); however, only 73% of its nominal capacity is governed in the push direction. It is confirmed by installed strain gages that indicated strain values were surpassed  $\xi_y$  during the test for the positive directions, while maximum strain in the negative direction reached about  $0.8 \xi_y$ . Thus, it can be concluded that slippage of smooth bars may prevent beams to reach their full nominal capacity. In other words, formation of plastic hinge in the beams (as it is expected in the modern designs) cannot be occurred in such sections. Aforementioned observations are summarized in Table 4 for the both tested exterior joint substructures.

The hysteretic behavior (relationship between drift and lateral force) and the effect of  $P-\Delta$  for both specimens are presented in Fig. 6. As it can be seen, SC1 exhibited a relatively high pinching effect and experienced rapid strength deterioration. The pinching may be attributed primarily to sliding of the smooth bars and shear failure in the joint region, while the strength reduction is mainly due to  $P-\Delta$  effect (see Fig. 6a). The latter can be explained by the observed damage status, which experienced wide cracks divided



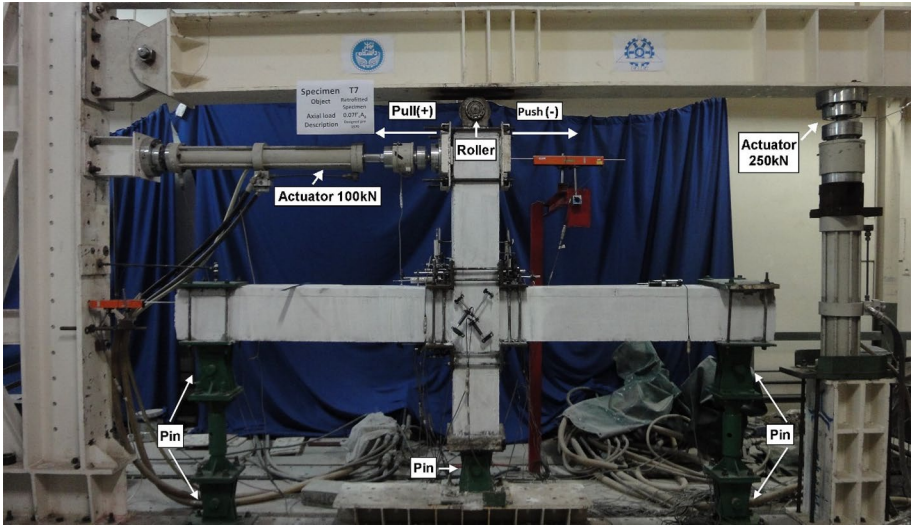


Fig. 3 Overview of test setup and instrumentation

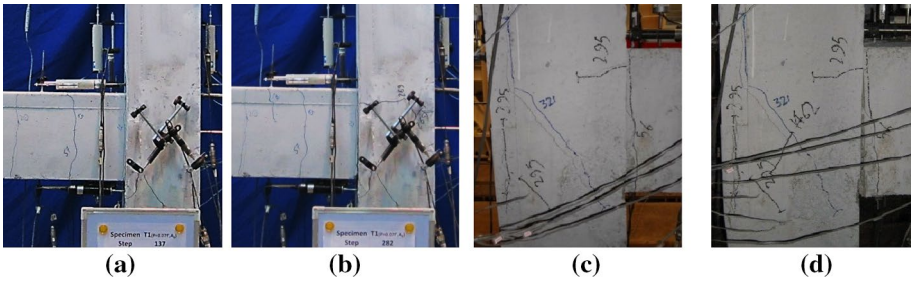


Fig. 4 Damage progression and crack observation for control Specimen SC1. a Drift 0.9%. b Drift 1.8%. c Drift 2.7%. d Drift 3.6%

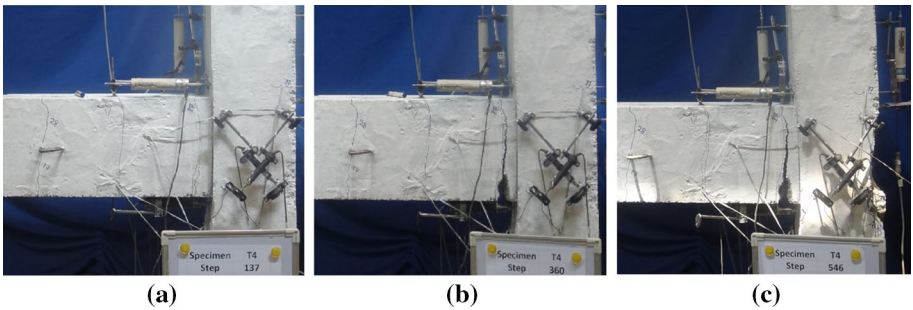
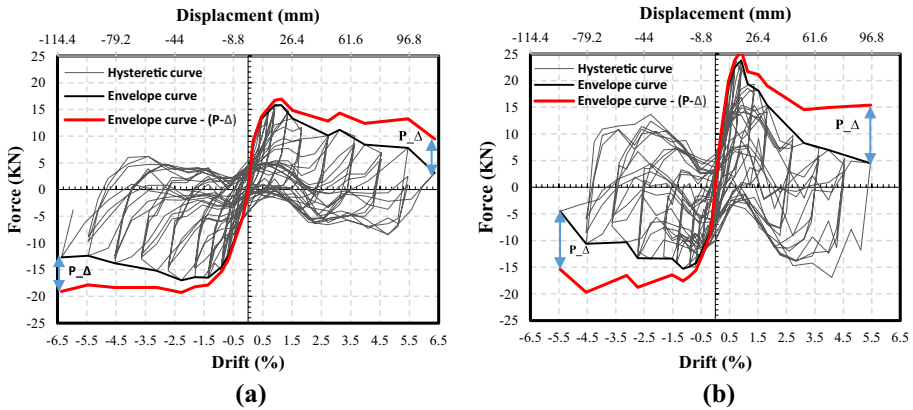


Fig. 5 Damage progression and crack observation for control Specimen SC1-1. a Drift 0.9%. b Drift 2.7%. c Drift 4.5%

**Table 4** Peak test load and ductility of exterior joints in both positive (pull) and negative (push) directions

Specimen	Peak load (kN) $F_y$		Drift at the yield point $\Delta_y$ (%)		Ultimate drift $\Delta_u$ (%)		Ductility factor $\mu$					
	Pull (+)	Push (-)	Average	Pull (+)	Push (-)	Average	Pull (+)	Push (-)				
SC1	15.8	-17	16.4	0.49	-0.95	0.72	1.99	-4.67	3.33	4.08	4.937	4.51
SC1-1	23.8	-15.3	19.55	0.57	-0.58	0.57	1.35	-2.87	2.11	2.38	4.95	3.67

$\delta_u$ : drift at either 20% drop of peak load, buckling of longitudinal reinforcement, fracturing of longitudinal or transverse reinforcement (whichever occurs first)



**Fig. 6** Hysteretic behavior, P-Δ effect, and backbone curve of the exterior joints (SC1 and SC1-1). **a** Specimen SC1. **b** Specimen SC1-1

the beam into a few solid segments and consequently, caused these segments to fluctuate under cyclic action.

The hysteretic curve of SC1-1 (the specimen with the higher axial load ratio) shows a relatively similar response to the SC1; however, it reached higher flexural capacity (about 50% in the pull direction) and experienced more radical strength deterioration than the sub-assembly with the lower axial load ratio. This strength reduction is mainly due to larger secondary effects (P-Δ) in this specimen due to existence of a higher axial load ratio. Furthermore, the specimen did not develop full nominal flexural capacity under the push direction, exactly like Specimen SC1.

### 3.2 Interior beam–column joint (SC2)

In this section, the observed seismic response of the interior joint (SC2) is summarized. In this regard, Fig. 7 illustrates the development of flexural cracks at different lateral loading levels. Similar to the exterior joints, the specimen cracked at very small lateral deformations (drift ratio of about 0.2%), which initially formed at the intersection of the left-side beam with the column and also at a distance of 11 cm from the column face in the right beam. Observed behavior led to conclude that SC2 remained linear up to larger

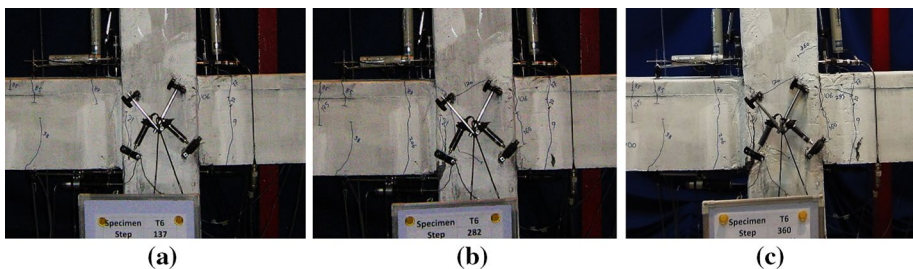


**Fig. 7** Damage progression and crack observation for the interior joint (SC2). **a** Drift 0.9%. **b** Drift 1.8%. **c** Drift 2.7%

deformation levels than the exterior joint with an identical axial load ratio (i.e. SC1). In the following, cracks parallel to longitudinal bars developed in the beam and concrete cover spalled at the joint region at a drift ratio of about 1.35%. Later, flexural cracks appeared in the top column and at a drift ratio of about 2.7%, whereas no crack was observed in the columns of exterior subassembly. In spite of such cracks, no serious damage was occurred in the columns, though the beams were stronger than them. Furthermore, the crack pattern over the beam did not vary significantly, no diagonal crack was observed in the joint panel zone, and the response of substructure was controlled by rocking behavior. It is worthwhile to note that the width of intersectional crack in SC2 was about 2 mm, which was much less than the corresponding value in the SC1 (about 5 mm). It can be interpreted as less slippage of longitudinal bars in the interior joint than that of the exterior joint due to continuity of them over the beam. Moreover, it presented a much more stable hysteretic behavior (smoother post-peak behavior) accompanied by more distributed cracks than the corresponding exterior joint. Similarly to the exterior subassemblies, development of wide cracks divided the interior substructure into a few solid blocks, which led to occurrence of large  $P-\Delta$  effects. In sum, the captured key response parameters of the SC2 are summarized in Table 5.

Hysteresis behavior of SC2 is presented in Fig. 8. As it can be seen, it shows an identical response in both directions (push or pull) due to its symmetric geometry; however, its full nominal flexural capacity did not develop. In other words, it reached to an average lateral load of 25.1 kN, which is about 81% of its nominal capacity (calculated as 31.1 kN). Moreover, specimen SC2 has smoother post-peak behavior than exterior specimens, i.e. it experiences gradual strength deterioration with increasing displacement in cyclic response. This situation may be explained by the low captured sliding in this case and also by the absence of any diagonal shear cracks in its joint region.

#### 4 Proposed nonlinear model for joint response

In this section, observed seismic responses of the interior and exterior joints in previous section are employed to propose a novel nonlinear model. In this regard, the schematic mechanisms of the main developed crack patterns for the both considered substructures are depicted in Fig. 9. As it is evident, the dominant damage mode in these substructures includes a deep crack at the intersection of the beam with the joint panel zone. Thus, cracking throughout beams/columns are negligible and diagonal cracking in the joint region is not crucial (Adibi et al. 2017a, b); which is completely different from observed failure modes of substructures reinforced by deformed bars.

Taking aforementioned failure modes into account, led a nonlinear rotational spring (a zero-length element) to be introduced at the intersection of the beams with the joint panel zone to model nonlinear behavior of such subassemblies (see Fig. 10) which is mostly governed due to bar slippage (see Fig. 11). In this approach, linear elastic beam–column elements are assigned to beams/columns; which is due to minor cracks observed during the experimental program. This assumption decreases the number of elements and consequently, reduces the computational costs. Furthermore, the geometry of the joint is modeled by rigid elements. This modeling strategy is presented in Fig. 10.

In the following, OpenSees software framework is used to construct corresponding nonlinear models of the tested subassemblies, following discussed strategy. In this regard, Pinching 4 constitutive model (see Fig. 12) available in the library of the software is employed to define

**Table 5** Peak test load and ductility of interior joint in both positive (pull) and negative (push) directions

Specimen	Peak load (kN) $F_y$		Drift at the yield point $\Delta_y$ (%)		Ultimate drift $\Delta_u$ (%)		Ductility factor $\mu$					
	Pull (+)	Push (-)	Average	Pull (+)	Push (-)	Average	Pull (+)	Push (-)				
SC2	27.7	22.5	25.1	1.47	1.59	1.53	5.50	6.20	5.85	3.73	3.90	3.82

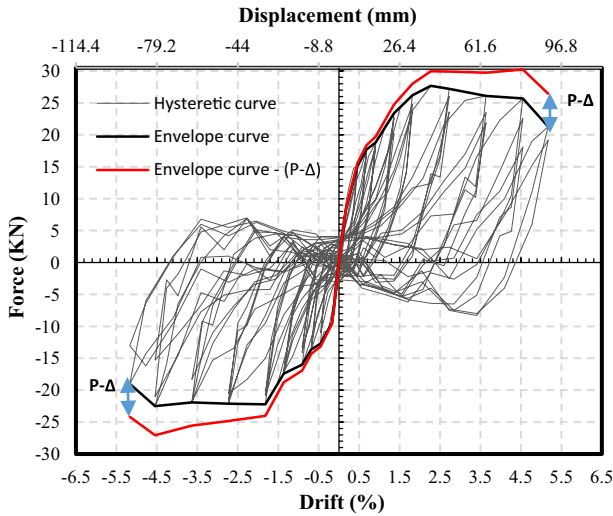


**Fig. 8** Hysteretic behavior, P-Δ effect, and backbone curve of the interior joint (SC2)

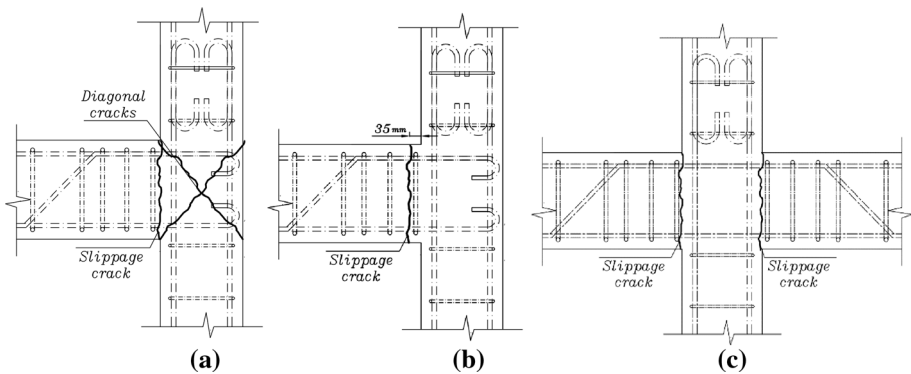


**Fig. 9** Schematic mechanism of developed cracks for the exterior and interior joint specimens. **a** Specimen SC1. **b** Specimen SC1-1. **c** Specimen SC2

nonlinear behavior of the spring at the critical section of the beam. It should be noted that the characteristics of this spring are defined based on the section properties of the adjacent beam (i.e.  $M-\theta$ ). Hence, envelop of the experimentally captured hysteresis curve of the adjacent beams (see Fig. 13) was employed to extract the required defining parameters of the nonlinear spring. It is worthwhile to note that rotation of the beam at each step of the test is calculated using recorded vertical displacements by two installed LVDTs (see Fig. 14) and Eq. 1. Additionally, the moment at the end of the beam is analytically evaluated using the applied lateral load at each step of the test.

$$\theta = \frac{\Delta_{LVDT1} - \Delta_{LVDT2}}{d} \tag{1}$$

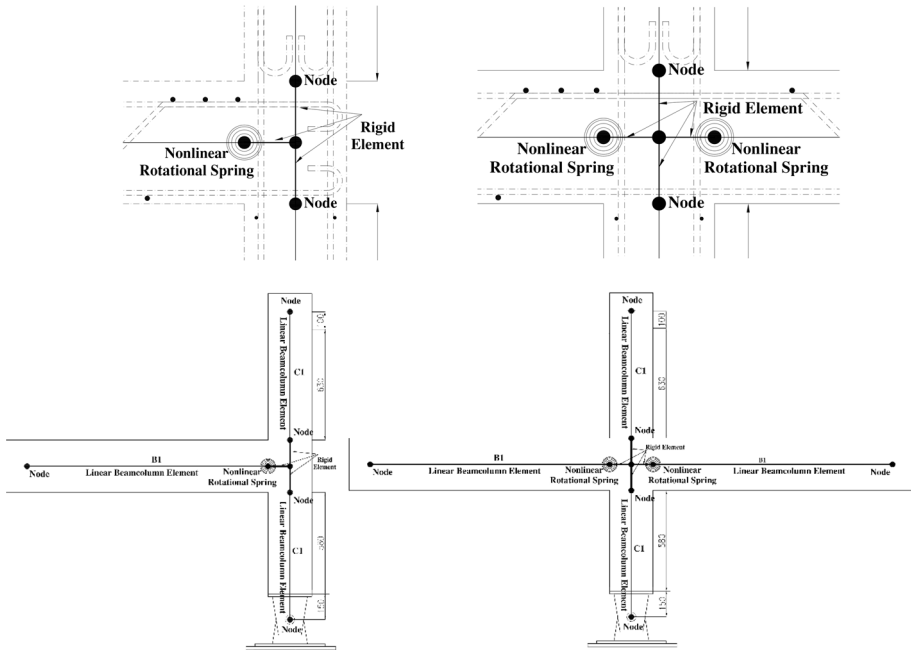


**Fig. 10** Proposed model for the exterior and interior joint substructures reinforced by plain bars

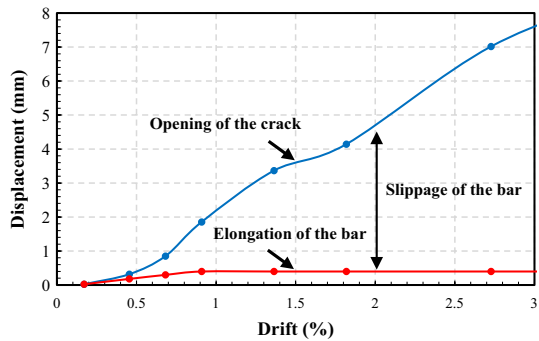


**Fig. 11** Opening of the crack at the intersection of the beam and column

As it can be seen in Fig. 12, nominal moment capacity of the adjacent beam controls discussed hysteretic moment-rotation behavior in both directions and is a function of its reinforcing detail. Therefore, this  $M-\theta$  behavior is assigned to the nonlinear spring of the proposed model to validate its applicability in modeling RC components reinforced by plain bars. The numerical response of SC1 is compared with experiment in Fig. 15. A relatively good agreement may be observed in such parameters as initial stiffness, unloading/reloading stiffness, and amount of dissipated energy. A transient increase in lateral load is observed in the positive direction (pull) of the experimental behavior. This is not predicted

**Fig. 12** Pinching 4 constitutive model (OpenSees 2013)

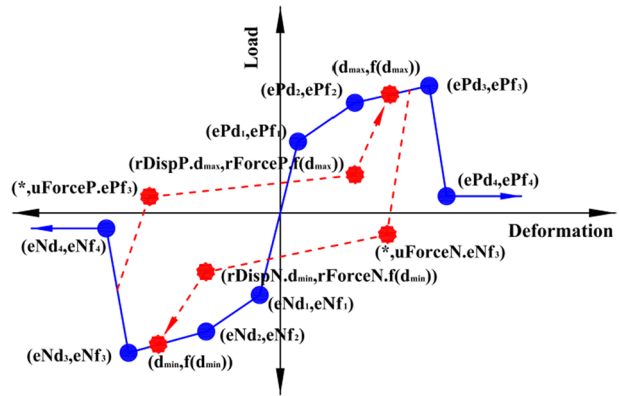


**Fig. 13** Hysteresis curve of  $M-\theta$  at the end section of the beam

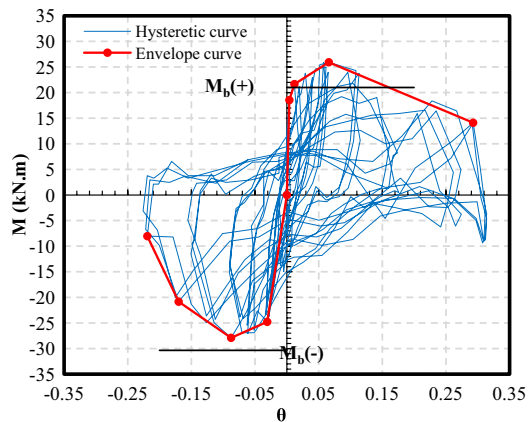
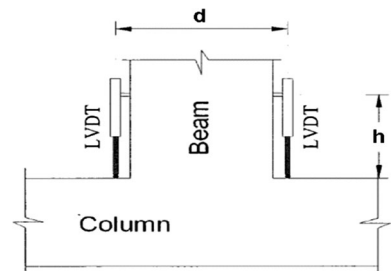


**Fig. 14** Evaluation of beam rotation with respect to the column

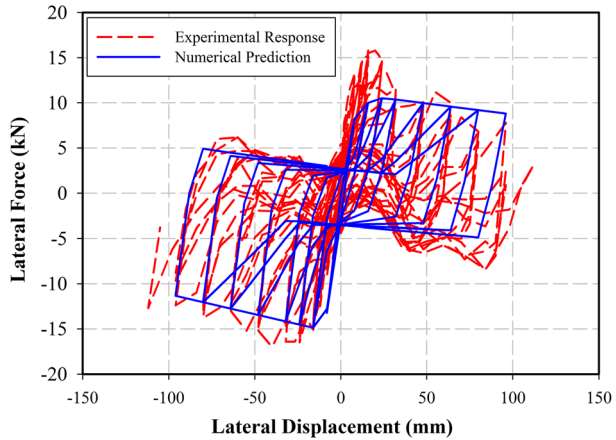


by the proposed model. This phenomenon may be attributed to induced confinement by axial load of the column. Nevertheless, this difference is in the conservative side for the numerical model, and may be neglected from the view point of professional design.

As it was previously discussed, the substructure is mainly damaged at the end of the beam (intersecting with the joint panel zone). Furthermore, it was shown in Fig. 15 that assigning a nonlinear spring with  $M-\theta$  behavior of the adjacent beam to the intersection of the beam with the joint can precisely predict the seismic response of the RC substructures reinforced by plain bars. Hence, an empirical constitutive model is proposed following



**Fig. 15** Comparison between simulated response of SC1 exterior beam–column joint and its experimentally captured behavior



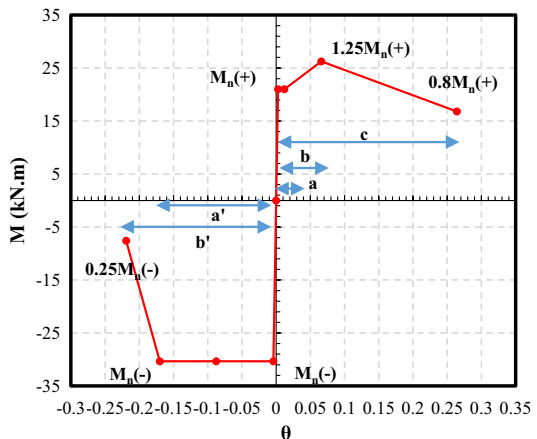
mentioned strategy to simulate exterior joints, which is detailed in Fig. 16. Elastic deformation of the spring is represented by the elastic rotation of the beam. Thus, yield rotation can be calculated by Eq. (2). It should be noted that no modification factor is assigned to the moment inertia of beams/columns. This assumption is due to observed failure mode of the desired subassemblies; however, regulations such as FEMA-356 (2000) and ASCE 41 (2007) (see Fig. 17) have proposed reducing modification factors (less than 1) for such objectives.

$$\theta_y = \frac{M_b L_b}{EI_b} \tag{2}$$

where,  $M_b$ ,  $L_b$ ,  $E$  and  $I_b$  are flexural moment, length, modulus of elasticity and moment inertia of the adjacent beam, respectively.

Post-elastic deformations of the assigned spring are derived from experimental tests. In order to make them generally applicable, the plastic deformations (i.e. deformation at each step minus yield deformation) are presented in Table 6.

**Fig. 16** Proposed nonlinear-model for the exterior joints with low axial load ratio



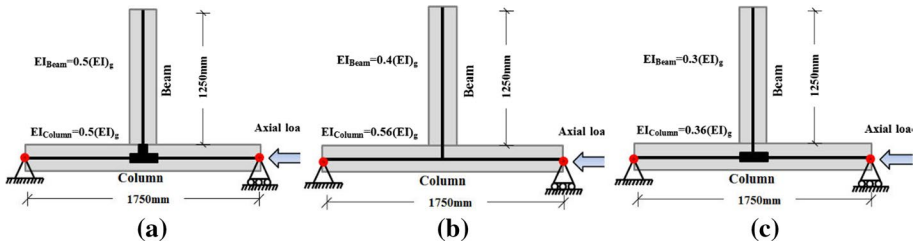


**Fig. 17** Modeling strategy of external substructures in different seismic design regulations or suggestions

**Table 6** Plastic deformations of the spring proposed for modeling of exterior beam–column joints with low axial load ratio

a (rad)	b (rad)	c (rad)	a' (rad)	b' (rad)
0.009	0.063	0.264	0.166	0.215

**Table 7** Comparison between simulated hysteretic parameters of the exterior beam–column joint with lower axial load ratio

Beam–column joint		Ultimate moment capacity (kN)		Initial cyclic stiffness (kN/mm)	Dissipated energy (kN mm) Up to drift 4.5%	Axial load level
		Direction+	Direction–			
Exterior joint	Tested spec SC1	15.8	– 17	2.28	10,568	$0.07A_g f'_c$
	Simulated spec SC1	11.0	14.9	2.23	10,120	

Finally, based on observed response of such subassemblies, the ultimate strengths of the spring were considered as 125 and 100% of the nominal moment capacity of the beam in positive and negative directions, respectively. Moreover, the failure state corresponds to a 20 and 75% reduction in nominal moment capacity of the beam respectively for the positive and negative directions.

In the following, the proposed model is employed to simulate the seismic response of the exterior beam–column joint with the low axial load ratio (SC1). Comparing obtained outcomes with those from experiment reveals accuracy of the proposed model. Cyclic behavior parameters of the tested and simulated exterior joints are compared in Table 6.

Additionally, a detailed investigation is carried out by comparing key parameters of the numerical prediction with experiment in Table 7. It is seen that the predicted moment capacities in positive and negative directions are about 70 and 80% of the experiment, respectively. These ratios for initial stiffness in positive and negative directions are about 95 and 90% of experimental stiffnesses, respectively. Moreover, the predicted dissipated energy until the drift ratio of 4.5% is about 95% of the measured value. Therefore, it can be concluded that the simulated parameters of cyclic behavior are almost close to that of the real values.

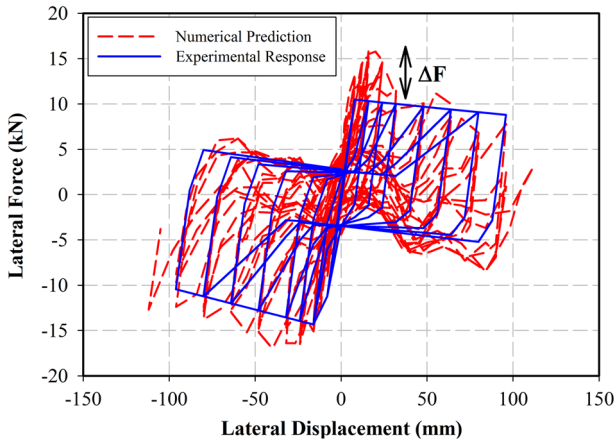
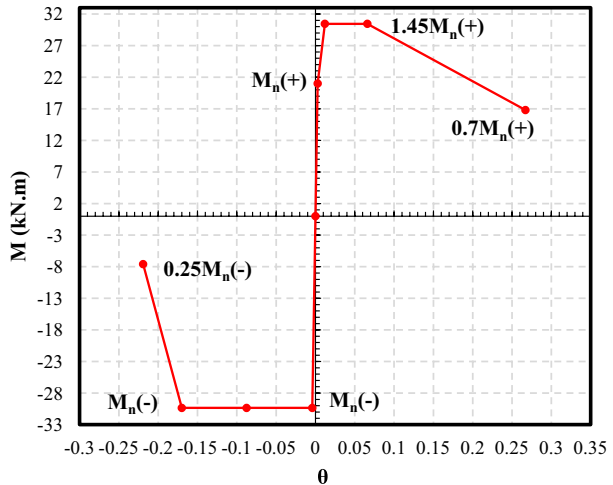


**Fig. 18** Evaluating accuracy of the proposed nonlinear model for exterior joints (SC1)

**Fig. 19** Proposed nonlinear model for the exterior joints with higher axial load ratio



### 5 Analytical verification of the proposed joint model

In this section, a same approach as previously discussed is followed to propose a nonlinear model for other tested beam–column joints, including exterior subassemblies with higher axial load ratio and also interior joints (Fig. 18).

Proposed model for the nonlinear spring of the exterior joint with higher axial load is presented in Fig. 19. This model is extracted from the experimental behavior of the SC1-1 specimen, which was detailed in Sect. 3.1. As it can be seen, the ultimate strength of the spring at the positive direction is about 145% of the nominal capacity of the adjacent beam. This increment with respect to the exterior joints with a lower axial load ratio is due to higher confinement level, which leads to reduction in bar slippage and crack development; however, the ultimate strength in negative direction remained unchanged. The calculation procedure of deformation capacities is discussed in previous section, and it is recommended to use identical plastic deformations as reported in Table 5.

**Fig. 20** Comparison between real and simulated response of the exterior beam–column joint with higher axial load level (SC1-1)

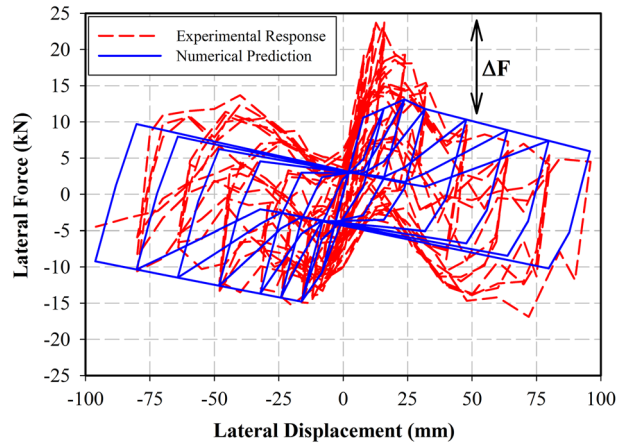


**Table 8** Comparison between simulated hysteretic parameters of the exterior beam–column joint with higher axial load ratio

Beam–column joint		Ultimate moment capacity (kN)		Initial cyclic stiffness (kN/mm)	Dissipated energy (kN mm) Up to drift 4.5%	Axial load level
		Direction+	Direction–			
Exterior joint	Tested spec SC1-1	23.8	– 15.3	2.42	18,500	$0.15A_g f'_c$
	Simulated spec SC1-1	13.5	– 15.0	2.38	17,450	

The proposed constitutive model in Fig. 19 is employed to simulate the response of the previously detailed exterior beam–column joint with higher axial load (SC1-1), which the comparison between numerically predicted response with corresponding experimental outcomes is presented in Fig. 20. As it is clear, the proposed model has been able to predict the capacity of the subassembly relatively well, however, it has failed to simulate the transient lateral capacity. The amount of this is about 30% of the substructure’s nominal capacity. This may be explained by strain hardening, higher confinement due to axial load of the column and using 180° hook at the end of longitudinal bars. As previously mentioned, the behavior of the substructure is controlled by the flexural capacity of the beam at the section adjacent to the joint panel zone and consequently, its capacity is a function of the longitudinal bars’ tensile strength, which its ultimate tensile strength can increase up to 40% of the nominal tensile strength due to strain hardening. It seems that some reasons such as more lateral spacing of the longitudinal bars in the beam section and using 180° hook caused longitudinal bars to develop their ultimate strength. More elaboration of this phenomenon requires further detailed investigation to be carried out in the future.

Similar to the pervious section, key simulated response parameters are compared with obtained experimental outcomes in Table 8. In this regard, the ultimate moment capacities of simulated substructure in positive and negative directions are about 56 and 98% of the ultimate capacity of the real subassembly, respectively. This ratio for the

simulated initial stiffness is about 98% of experimentally captured stiffness. Moreover, the predicted dissipated energy until the drift ratio of 4.5% is about 94% of the measured value.

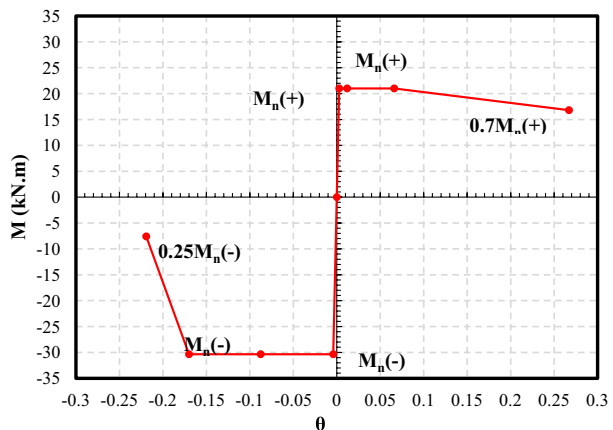
Finally, the proposed nonlinear model for the interior RC joints with low axial load and reinforced by plain bars is presented in Fig. 21. This model is extracted by following previously discussed methodology for the exterior joints by taking the experimental behavior of SC2 specimen into account. In this model, the ultimate capacity of the substructure equals to the nominal moment capacity of the adjacent beam. Hence, the ultimate capacity of the assigned spring in this case is decreased in comparison with the exterior joint with low axial load. It is due to the continuity of the longitudinal bars of the beam in the interior joint and absence of hoops in the joint panel (see Fig. 2).

Moreover, calculation procedure of the elastic rotations is similar to the previous cases, and it is recommended to adopt identical proposed plastic deformation in Table 5 for the post-elastic behavior.

The proposed model is employed to simulate the seismic behavior of the interior beam–column joint with low axial load (SC2), which its response was previously detailed in Sect. 3.2. Comparison between numerically predicted behavior with that of the experimentally observed one is depicted in Fig. 22. As it is evident, the simulated response matches well with the experimental outcomes, including cyclic behavior, ultimate moment capacity, initial stiffness and dissipated energy. The detailed comparison of these parameters is also reported in Table 9. As it can be seen, the ultimate moment capacities of simulated substructure in positive and negative directions are 97 and 95% of the corresponding values in the tested substructure, respectively. These ratios for the initial stiffness in positive and negative directions are 95 and 93%, respectively. Moreover, the numerical model led to a dissipated energy of about 95% of the experimentally measured value up to drift ratio of 4.5%.

On the other hand, contrary to exterior joint, no lateral transient capacity is noticed for the interior substructure. It may be related to absence of hoops for longitudinal bars within the joint panel that consequently, leads the ultimate moment capacity of the simulated and tested substructures to be relatively equal. Moreover, the bearing capacity of the substructure was developed gradually (slower than exterior joints) due to having continuous longitudinal bars in both top and bottom of the beam’s section which leads

**Fig. 21** Proposed nonlinear model for the interior beam–column joints with low axial load



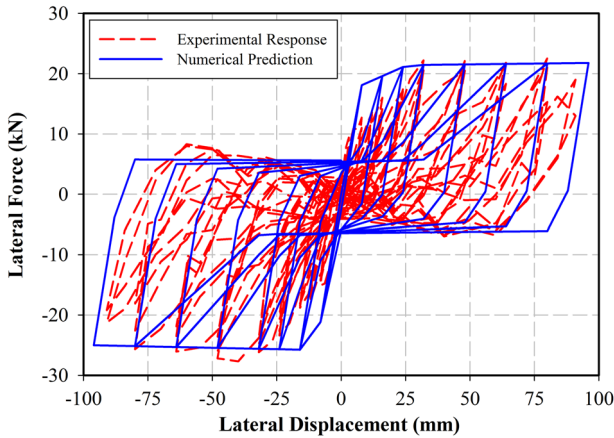


**Fig. 22** Comparison between real and simulated response of the interior beam–column joint with (SC2)

**Table 9** Comparison between simulated hysteretic parameters of the interior beam–column

Beam–column joint		Ultimate moment capacity (kN)		Initial cyclic stiffness (kN/mm)	Dissipated energy (kN mm) Up to drift 4.5%	Axial load level
		Direction+	Direction–			
Interior joint	Tested spec SC2	27.7	– 22.5	2.93	10,590	$0.07A_g f'_c$
	Simulated spec SC2	27.8	– 22.0	2.85	10,670	

them to slip. In other words, their slippage in the joint region causes the strength to be developed relatively slowly.

## 6 Scope and procedure of the proposed method

As previously discussed, several analytical modeling techniques have been proposed for simulating RC beam–column joints; while most of them are developed for components reinforced by deformed bars. Furthermore, test observations (Pampanin et al. 2000; Calvi and Pampanin 2002; Adibi et al. 2017a, b) highlighted the key differences (including controlling failure modes, capacities and ductility) between behavior of joints reinforced by deformed bars with those reinforced by plain bars. Such differences cause implementation of available models to be inaccurate in case of beam–column joints reinforced by plain bars.

Considering all, the current study aimed to propose a novel nonlinear constitutive model, which has some similarities with the model proposed by Calvi and Pampanin (2002). However, as it is shown in Fig. 23, the experienced shear strength for desired components of this article for both exterior and interior joints is reduced with respect to the proposed model by Calvi and Pampanin (2002), Adibi et al. (2017a). In addition, these

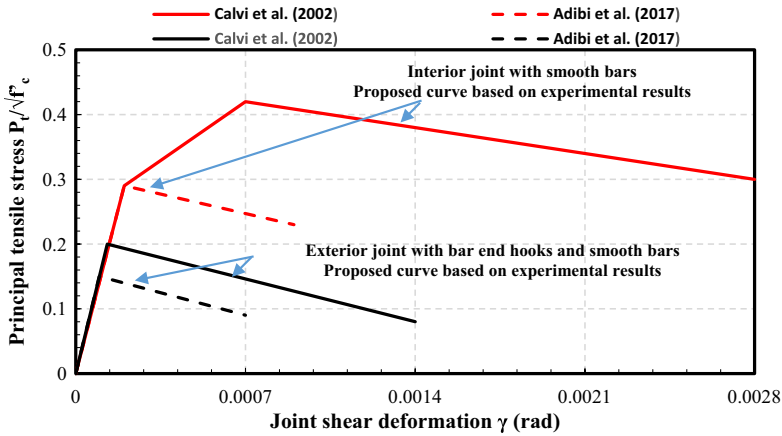


**Fig. 23** Shear degradation models for external joints (Calvi and Pampanin 2002; Adibi et al. 2017)

two types of joints had different damage patterns subjected to lateral loading. For instance, the seismic behaviors of the exterior beam–column joints tested by Calvi et al. were usually controlled by developing diagonal shear cracks in the joint panel (like substructures reinforced by deformed bars), while deep cracking at the intersection of beam and column (mostly dependent on the flexural capacity of the beam) was the dominant failure mode of the tested beam–column joints in this study.

Therefore, it is essential to distinguish applicability of each strategy. This is achieved by presented scope and procedure for both models in Fig. 24.

As it can be seen, it is required to evaluate initially the column’s horizontal shear force ( $V_c$ ) for estimation of the joint’s corresponding horizontal shear force ( $V_{jt}$ ). (see Fig. 25). Additionally, the flexural demand of the beam ( $M_b$ ) corresponded to the lateral force ( $P$ ) at the top of the column should be calculated by Eq. 2. Finally, the diagonal tension stress ( $f_t$ ) in the joint panel zone can be obtained by a combination of both its horizontal shear stress ( $v_{jt}$ ) and axial stress ( $f_a$ ) using Eqs. (5) and (6) (Fig. 26).

$$V_{JT} = T_1 - V'_C \quad (V'_C = P) \tag{3}$$

$$M_b = P * h * \frac{l}{l + 0.5b} \tag{4}$$

$$v_{jt} = \frac{V_{JT}}{b_j h_c} \tag{5}$$

$$f_t = -\frac{f_a}{2} + \sqrt{\left(\frac{f_a}{2}\right)^2 + v_{jt}^2} \tag{6}$$

Finally, the proposed model in the current study is compared with that of the Calvi et al., which is one of the well-known modeling strategies for RC components reinforced by plain bars in the literature (see Fig. 27). As previously discussed, the method of Calvi et al. is developed for substructures mostly experiencing diagonal shear cracks at the joint

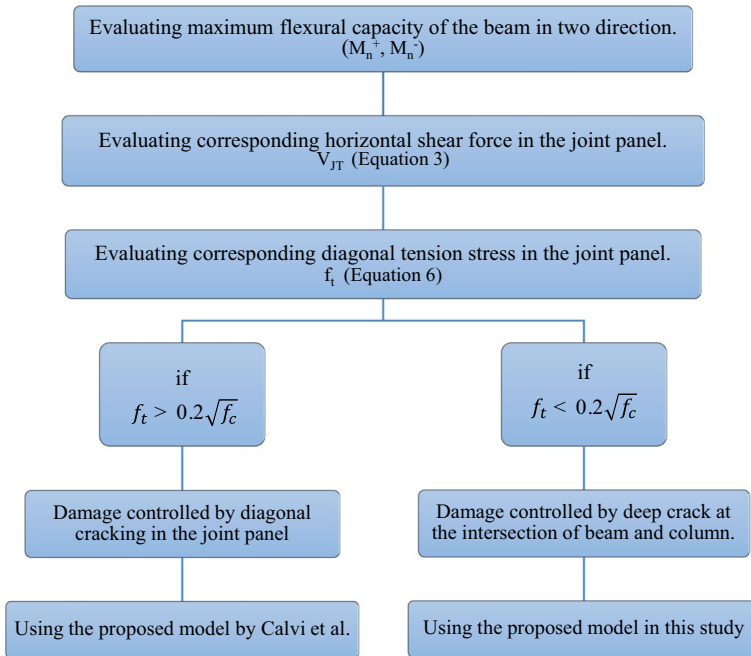
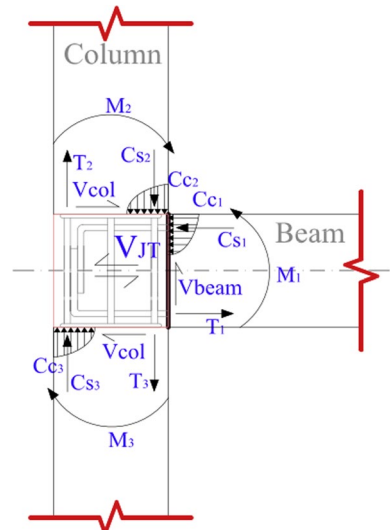


**Fig. 24** Scope and procedure of the proposed model versus that of the Calvi et al.

**Fig. 25** Diagram of internal force in exterior joints



panel zone. For comparison objective, the obtained experimental outcome for the exterior beam–column joint specimen with high axial load (SC1-1) is considered. It is worthwhile to note that an elastic–perfectly plastic constitutive law and nonlinear beam–column elements are assigned for the nonlinear spring of the joint and beams/columns, respectively.



**Fig. 26** Diagram of loading pattern in exterior joints

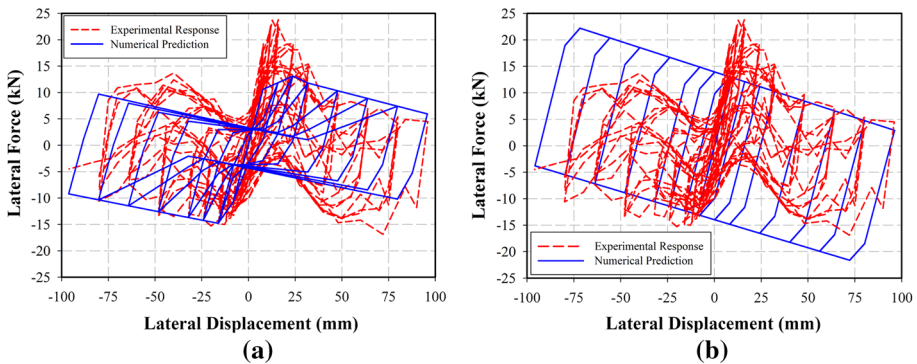
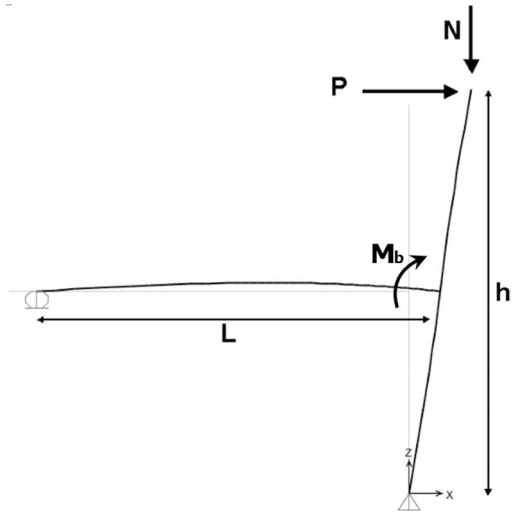


**Fig. 27** Comparison between different proposed nonlinear modeling methods of RC beam–column joints reinforced by plain bars using experimental response of SC1-1 (exterior substructure with high axial load ratio). **a** Proposed model in the current article. **b** Proposed model by Calvi et al.

As it is clear, both models cannot predict the lateral transient capacity; however, the captured capacities and initial stiffnesses are relatively in a same order. On the other hand, the most important difference is related to the amount of dissipated energy, which highlights misleadingly prediction of Calvi et al.’s model for components with mostly slippage failure mode.

## 7 Conclusion

The current study was aimed to propose a reliable nonlinear modeling technique to be implemented in the seismic assessment of existing RC components reinforced by plain bars. In this regard, obtained database from surveying buildings constructed during 1970s is employed to design an extensive experimental program, which investigated cyclic behavior of both exterior and interior beam–column joints with different axial load levels. Later,

observed damage and failure modes were taken into account to develop both straightforward nonlinear modeling strategy and constitutive models. In sum, the obtained outcomes can be summarized as follows:

- A novel nonlinear modeling technique is proposed to capture the post-elastic behavior of reinforced concrete subassemblies with old-fashioned joints and plain bars. It is worthwhile to note that previous studies within this field focused on joints with dominant shear failure; however, the current article focused on beam–column connections with mostly bar slippage failure mode.
- A flowchart is introduced to distinguish between the dominant failure mechanisms (i.e. diagonal shear cracking at the joint panel zone or deep flexural cracking at the intersection of the beam with the joint) and to employ the proper modeling method. Based on that, the principal tensile strain at the joint panel zone can be used to determine which failure mode and consequently, the modeling strategy should be adopted.
- The proposed model consists of a linear elastic beam–column element which is assigned to beam/column components of the substructure and rigid elements which are used to consider the geometry of the joint. Furthermore, a nonlinear rotational spring (zero-length element) is introduced at the intersection of the adjacent beam with the joint panel zone to capture bar slippage inside the joint region. In other words, the nonlinear behavior of the substructure is considered to be governed only by large deformations arising from slip of longitudinal plain bars.
- Nonlinear moment-rotation behavior of the assigned springs is defined by nominal moment capacity of the adjacent beam and reinforcement details of the joint region. Thus, the yield moment of the joint is assumed to be equal to the nominal moment capacity of the beam; however, its ultimate capacity varies depending on configuration (being interior or exterior), axial load level and moment direction (positive or negative). In this regard, the ultimate moment capacity of exterior joints with low axial load and in positive direction was proposed to be 125% of the beam's nominal moment capacity. This value for the exterior joints with high axial load and interior joints is recommended to be 145% and 100%, respectively. It should be noted that the ultimate moment capacity in negative directions was limited to the nominal moment capacity of the beam. Moreover, a 20–30 and 75% moment capacity reduction was considered for the post-peak strength deterioration, respectively, for positive and negative directions. Regarding the deformations of the assigned spring, yield rotation of the adjacent beam is recommended, while no modification factor should be applied to its moment of inertia. Additionally, empirical plastic rotations are recommended to calculate post-elastic deformations.

## References

- Adibi M, Marefat MS, Esmaily A, Karbasi AK, Esmaily A (2017a) Seismic retrofit of external concrete beam–column joints reinforced by plain bars using steel angles prestressed by cross ties. *Eng Struct* 148:813–828
- Adibi M, Marefat MS, Karbasi AK, Zare H (2017b) External retrofit of beam–column joints in old fashioned RC structures. *Earthq Struct* 12(2):237–250
- Alath S, Kunnath SK (1995) Modeling inelastic shear deformations in RC beam–column joints. In: *Engineering mechanics proceedings of 10th conference, ASCE, University of Colorado at Boulder, Boulder, Colorado*, pp 822–825

- Allahvirzideh R, Gholipour Y (2017) Reliability evaluation of predicted structural performances using nonlinear static analysis. *Bull Earthq Eng* 15(5):2129–2148
- Allahvirzideh R, Mohammadi MA (2016) Upgrading equivalent static method of seismic designs to performance-based procedure. *Earthq Struct* 10(4):849–865
- Allahvirzideh R, Khanmohammadi M, Marefat MS (2017) Probabilistic comparative investigation on introduced performance-based seismic design and assessment criteria. *Eng Struct* 151:206–220
- Altoontash A (2004) Simulation and damage models for performance assessment of reinforced concrete beam–column joints. Stanford University, California
- ASCE, SEI 41 (2007) Seismic rehabilitation of existing buildings. American Society of Civil Engineers, Reston
- ATC (1989) A handbook for seismic evaluation of existing buildings ATC-22. Applied Technology Council, Redwood City
- Barker JA (1979) Reinforced concrete detailing, vol Second. Oxford University Press, London (**1st printed at 1967**)
- Bedirhanoglu I, Ilki A, Pujol S, Kumbasar N (2010) Behavior of deficient joints with plain bars and low-strength concrete. *ACI Struct J* 107(3):300
- Biddah A, Ghobarah A (1999) Modelling of shear deformation and bond slip in reinforced concrete joints. *Struct Eng Mech* 7:413–432
- Braga F, Gigliotti R, Laterza M (2009) RC existing structures with smooth reinforcing bars: experimental behaviour of beam–column joints subject to cyclic lateral loads. *Open Const Build Technol J* 3:52–67
- Braga F, Gigliotti R, Laterza M, D’Amato M, Kunnath S (2012) Modified steel bar model incorporating bond-slip for seismic assessment of concrete structures. *J Struct Eng* 138(11):1342–1350
- Calvi GM, Pampanin S (2002) Relevance of beam–column joint damage and collapse in RC frame assessment. *J Earthq Eng* 6(1):75–100
- Calvi GM, Magenes M, Pampanin S (2001) Experimental study on the seismic response of RC frame designed for gravity loads only. In: Proceedings of the 10th Italian national conference on earthquake engineering (ANIDIS), Potenza-Matera (**In Italian**)
- Cosenza E, Prota A (2006) Experimental behaviour and numerical modelling of smooth steel bars under compression. *J Earthq Eng* 10(3):313–329
- D’Amato M, Braga F, Gigliotti R, Kunnath S, Laterza M (2012) Validation of a modified steel bar model incorporating bond-slip for seismic assessment of concrete structures. *J Struct Eng* 138(11):1351–1360
- Del Vecchio C, Di Ludovico M, Balsamo A, Prota A (2017) Seismic retrofit of real beam–column joints using fiber reinforced cement (FRC) composites. *J Struct Eng Press*. [https://doi.org/10.1061/\(ASCE\)ST.1943-541X.0001999](https://doi.org/10.1061/(ASCE)ST.1943-541X.0001999)
- Duhman CW (1953) The theory and practice of reinforced concrete. McGraw-Hill, New York
- Edvard NJ, Tanner JL (1996) Theory and problems of reinforced concrete design. Schaum Publishing co., New York
- El-Metwally SE, Chen WF (1988) Moment rotation modeling of reinforced-concrete beam–column connections. *ACI Struct J* 85:384–394
- FEMA-356 (2000) Prestandard and commentary for the seismic rehabilitation of buildings. Federal Emergency Management Agency, Washington, D. C.
- Giberson MF (1969) Two nonlinear beams with definition of ductility. *J Struct Div ASCE* 95:137–157
- Guerrin A (1959) *Traite De Beton Arme*. Dunod, Paris
- Hakuto S, Park R, Tanaka H (1995) Retrofitting of reinforced concrete moment resisting frames, research report 95-4. Department of Civil Engineering, University of Canterbury, Canterbury
- Hakuto S, Park R, Tanaka H (1999) Effect of deterioration of bond of beam bars passing through interior beam–column joints on flexural strength and ductility. *ACI Struct J* 96(5):858–864
- Hakuto S, Park R, Tanaka H (2000) Seismic load tests on interior and exterior beam–column joints with substandard reinforcing details. *ACI Struct J* 97(1):11–25
- Laterza M, D’Amato M, Gigliotti R (2017) Modeling of gravity-designed RC sub-assemblages subjected to lateral loads. *Eng Struct* 130:242–260
- Liu A, Park R (2000) Seismic behavior of existing moment-resisting frames with plain round reinforcing bars designed to pre-1970s codes. In: Proceeding of 12th world conference on earthquake engineering
- Liu A, Park R (2001) Seismic behaviour and retrofit of pre 1970’s as built exterior beam–column joint reinforced by plain bars. *Bul N Z Soc Earthq Eng* 34(1):68–81
- Lowes L, Altoontash A (2003) Modeling reinforced-concrete beam–column joints subjected to cyclic loading. *J Struct Eng* 129:1686–1697
- Manfredi G, Verderame GM, Lignola GP (2008) A FEM model for the evaluation of the seismic behavior of interior joints in reinforced concrete frames. In: The 14th world conference on earthquake engineering; October 12–17, 2008, Beijing, China (paper ID: 05-01-0189)

- Marefat MS, Khanmohammadi M, Bahrani MK, Goli A (2005) Cyclic load testing and numerical modeling of concrete columns with substandard seismic details. *Comput Concrete* 2(5):367–380
- Marefat MS, Khanmohammadi M, Bahrani MK, Goli A (2006) Experimental assessment of reinforced concrete columns with deficient seismic details under cyclic load. *Adv Struct Eng* 9(3):337–347
- OpenSees (2013) Open system for earthquake engineering simulation, Pacific Earthquake Engineering Research Center, University of California, Berkeley CA, <http://opensees.berkeley.edu/>
- Otani S (1974) Inelastic analysis of RC frame structures. *J Struct Div ASCE* 100:1433–1449
- Pampanin S, Calvi GM, Moratti M (2000) Seismic behaviour of R.C. beam–column joints designed for gravity loads. In: *Proceeding of 12th European conference on earthquake engineering*
- Pampanin S, Magene G, Carr A (2003) Modelling of shear hinge mechanism in poorly detailed RC beam–column joints. In: *Proceedings of the fib symposium concrete structures in seismic Regions*. Athens
- Pampanin S, Christopoulos C, Chen T-H (2006) Development and validation of a metallic haunch seismic retrofit system for existing under-designed RC frame buildings. *J Earthq Eng Struct Dyn* 35:1739–1766
- Park R (2002) A summary of results of simulated seismic load tests on reinforced concrete beam–column joints, beams and columns with substandard reinforcing details. *J Earthq Eng* 6(2):147–174
- Park R et al (1995) The Hyogo-ken Nanbu earthquake (The Great Hanshin Earthquake) of 17 January 1995. Report of the NZNSEE Reconnaissance Team. *Bull N Z Nat Soc Earthq Eng* 28(1):1–98
- Pernot P (1954) *Le Beton Arme*. J. B. Balliere et Fils, Editeurs
- Russo G, Pauletta M (2012) Seismic behavior of exterior beam–column connections with plain bars and effects of upgrade. *ACI Struct J* 109(2):149
- Sezen H, Elwood KJ, Whittaker AS, Mosalam KM, Wallace JW, Stanton JF (1999) *Structural Engineering Reconnaissance of the August 17, 1999 Earthquake: Kocaeli (Izmit), Turkey*, PEER Report 2000/09. University of California, Berkeley
- Sezen H, Whittaker AS, Elwood KJ, Mosalam KM (2003) Performance of reinforced concrete buildings during the August 17, 1999 Kocaeli, Turkey earthquake, and seismic design and construction practice in Turkey. *Eng Struct* 25:103–114
- Soleimani D, Popov EP, Bertero VV (1979) Hysteretic behavior of reinforced concrete beam–column subassemblages. *ACI Struct J* 76(11):1179–1195
- Taylor FW, Thompson SE, Smulski E (1925) *Concrete plain and reinforcement*, vol 4. Wiley, New York
- Youssef M, Ghobarah A (2001) Modelling of RC beam–column joints and structural walls. *J Earthq Eng* 5:93–111
- Yurdakul O, Avsar O (2016) Strengthening of substandard reinforced concrete beam–column joints by external post-tension rods. *Eng Struct J* 107:9–22